Mercury Porosimetry and X-ray Microtomography for 3-Dimensional Characterization of Multilayered Paper: Nanofibrillated Cellulose, Thermomechanical Pulp, and a Layered Structure Involving Both

Mohamed Ali Charfeddine,[a] Jean-Francis Bloch,[b,*] and Patrice Mangin [a]

Mercury intrusion porosimetry (MIP) is an inexpensive and common technique to characterize porous structures like paper. One major limitation of MIP is the lack of information about the arrangement of pores in the structure, information that is particularly relevant for multilayer structures such as thickness-structured paper. In this article, results from Synchrotron X-ray 3D microtomography are combined with MIP data to provide in-depth and improved information about the structures.

Keywords: Mercury intrusion porosimetry; Synchrotron X-ray 3D microtomography; Porosity profile; Bulk porosity; Surface porosity

Contact information: a: Lignocellulosic Materials Research Center, 3351, boul. des Forges, C.P. 500, Trois Rivières, Canada; b: Univ. Grenoble Alpes, CNRS, Grenoble INP, 3SR, F-38000 Grenoble, France; *Corresponding author: jean-francis.bloch@3sr-grenoble.fr*

INTRODUCTION

Mercury intrusion porosimetry (MIP) is a common technique for the analysis of the structure of porous materials (Johnson *et al.* 1999), which allows the characterization of a wide range of pore sizes from the microscale (500 µm) up to the nanoscale (3 nm). The technique provides structural parameters such as porosity, pore volumes, pore size distribution, density, and specific surface (Giesche 2006). Moura *et al.* (2005) showed that MIP is suitable to detect structural differences in paper structures. Bloch and Kedadi (2001) established that the MIP technique is efficient also to characterize the structure of a porous medium displaying porosity gradients, such as a paper. MIP has been widely used to characterize the structure of coated paper with micro- or nanofibrillated cellulose (MNFC) (Hamada *et al.* 2010; Ridgway and Gane 2013; Dimic-Misic *et al.* 2014). However, MIP cannot provide information about the pore shapes or about the spatial pore distribution in the paper structure. To overcome such shortcoming, MIP measurements are usually coupled with scanning electron images (SEM) to link observed variations in the MIP curves to the SEM pictures of pore shape and diameter in the paper structure (Yamauchi 2007; Zauer *et al.* 2014). Similar research has also been carried out for other materials, such as cement (Abell *et al.* 1999). Some shortcomings of the comparison of the mercury intrusion and 2D analysis have been described; for example, complementary experimental characterizations such as SEM have been used (Munch and Holzer 2008). Simulations of the evolution of the capillary pressure on a paper were presented (Hyväluoma *et al.* 2007) based on microtomography. This simulation aspect is not the scope of our work, rather our study is dedicated to the characterization of multilayered papers.

High-resolution Synchrotron X-ray 3D microtomography (SµT) has shown its capacity to analyze the paper structure (Rolland du Roscoat *et al.* 2005; Holmstad *et al.*

2006). Besides the visualization of the internal structure of the paper, various structural parameters such as porosity, specific surface area, and anisotropy are obtained by further image treatment. In addition, SμT can provide the spatial pore and filler distribution in the paper structure (Rolland du Roscoat *et al.* 2012). Paper-based composites were also studied successfully (Considine *et al.* 2010). Recently, SμT was used to characterize the z-structured paper by the layered addition of the MNFC (Charfeddine *et al.* 2016).

The MNFC was supplied by Omya International AG (Oftringen, Switzerland). It was obtained from a mix of bleached eucalyptus pulp with ground calcium carbonate (Hydrocarb®50, Omya) in the ratio of 80% cellulose and 20% mineral, which are combined during the manufacture of the MNFC. The mixture at a consistency of 2.72% was heated to 96 °C before being pumped, for a total of three passes, through a pilot scale homogenizer (LPN 500 from GEA Niro Soavi). The pressure drop was fixed at 600 bars. The obtained MNFC has a diameter ranging from 20 nm (nano-part) to 15 μm (micro-part) and a length of up to 1 mm. For papermaking, the MNFC suspension was diluted to a concentration of 0.1 wt% fibrils. In order to understand the effects of the MNFC layer inclusion, the z-structures were obtained considering two positions in depth, namely the top and middle of the sheet. The basis weight of the MNFC layers was varied from 2 to 20 $g \cdot m^{-2}$. The total basis weight of the z-structured sheets for all sheets was 60 $g \cdot m^{-2}$, indicating no measurable loss of MNFC. A 100% TMP sheet, also at 60 $g \cdot m^{-2}$, and a 100% MNFC sheet at 40 $g \cdot m^{-2}$ served as references. After wet formation, the sheets were pressed at 2, 3, and 4 bars between two blotting papers before drying at 105 °C for 10 min.

The technique proved to be efficient constituting a well-performing tool to identify MNFC location in the paper structure. Furthermore, 3D tomography porosity profiles in the paper thickness confirmed the retention of MNFC in the paper structure and the creation of the targeted layered structures. Nevertheless, the access to SμT measurements is limited due to the high cost and up-to-date technology needed. Thus, the aim of the present article is to pair results from SμT with results from MIP to improve overall MIP data analysis, and also to improve the structural characterization of such paper structures.

EXPERIMENTAL

Paper Samples

The paper samples used were a 100% TMP sheet (the reference) with a basis weight of 60 $g \cdot m^{-2}$ and 100% MNFC film with a 40 $g \cdot m^{-2}$ basis weight. The third sample is a z-structured paper obtained by the addition of an MNFC film in the middle of to the TMP sheet to constitute a layered structure. A MNFC layer of 6 $g \cdot m^{-2}$ is added in the middle of thickness of the paper during sheet formation. The final basis weight of the z-structured paper is kept constant at 60 $g \cdot m^{-2}$. All paper samples are made at laboratory scale using the Dynamic Sheet Former (DSF). Further details about the raw materials and the papermaking condition can be found in (Charfeddine *et al.* 2016).

Methods

Mercury intrusion porosimetry

Mercury is a non-wetting liquid. In the method, pressure is applied to force mercury to penetrate into the porous material. By increasing the pressure, the mercury fills smaller pores according to the following Laplace relation,

$$\Phi = - (4 \gamma \cos \theta)/P \quad (1)$$

where γ is the surface tension and θ is the contact angle of mercury with the material to be tested. Φ is the mean equivalent pore diameter and P is the applied pressure.

MIP measurements were performed using an Autopore IV mercury porosimeter (Micromeritics) that allows a maximum applied pressure of 207 MPa (30,000 PSI) corresponding to pore diameters about 7 nm. To avoid air pocket formation, the samples of 2 x 10 cm^2 were prepared according to the method described in Ridgway and Gane (2003) before being installed in the penetrometer. All MIP data were corrected to the expansion of the penetrometer. The specific surface area S_v was then calculated from the pore volume curves using the equation obtained easily from the one published earlier (Rootare and Prezlow 1967),

$$S_v = 4/\varepsilon \sum (d\varepsilon/\Phi)_i \quad (2)$$

where ε is the porosity and Φ is the pore diameter.

X-ray Synchrotron microtomography

The 3D images were obtained in the ID19 beamline of the European Synchrotron Radiation Facilities (ESRF) located in Grenoble (France). A pixel size of 0.65 µm was selected to lead to a field of view of 1.4 × 1.4 × paper thickness (e) mm^3. The sample, fixed on a rotating stage, was irradiated by the X-ray beam. The transmitted beam was recorded using a high-resolution camera. A detailed description of the experimental set-up can be found in (Rolland du Roscoat *et al.* 2005; Charfeddine *et al.* 2016).

From the X-ray images, the paper porosity and the specific surface were calculated using Avizo 3D software (FEI corporated software). In 3D images, porosity is defined as the ratio of the number of voxels in the porous region by the total voxel number of the image. The specific surface is then calculated by dividing the fibers surface by the fibers volume. The mean pore diameter of the paper is calculated using the Tomkieff relation reported by Bloch and Rolland du Roscoat (2009),

$$\langle \Phi \rangle = 4\varepsilon / S_v \quad (3)$$

where Φ is the mean pore diameter of the paper, S_v is the specific surface of the paper, and ε is the global paper porosity.

RESULTS AND DISCUSSION

Mercury Porosimetry

Figure 1 shows typical pore volume curves obtained from MIP. The difference between the 100% TMP sheet and the 100% MNFC film curves reflects the difference in the sample structure. MNFC film has a low cumulative pore volume of 0.4 $cm^3 \cdot g^{-1}$ when compared to the reference TMP sheet at 1.5 $cm^3 \cdot g^{-1}$. Such a low pore volume is expected, since many studies already reported the capacity of MNFC to form a dense structure with low porosity (Brodin *et al.* 2014). Furthermore, the difference in the structure between the TMP sheet and the MNFC film can be easily appreciated in the differential pores volume curves. We consider that the single peak at 1 µm in the MNFC curve represents the average porosity between the MNFC fibrils. However, the TMP curve presents two peaks: a peak at 8 µm and a second one at 3 µm. According to Zauer *et al.* (2014), the pores ranging from

10 nm to 5 µm are considered as microvoids in the paper structure. They include the pointed end of lumens, pit apertures, and membrane voids. Thus, the peak at 8 to 9 µm represents the voids between the TMP fibers and the peak at 3 µm is related to the lumen fiber volume accessible from the fiber wall pits, as explained by Moura and Figueiredo (2002). The addition of the MNFC layer to the TMP sheet reduced the total pore volume of the z-structured paper down to 1.29 $cm^3 \cdot g^{-1}$. It is notable that the MNFC addition does not impact the pores with a diameter above 10 µm as showed in the Fig. 1(a). The differential pore curve of the z-structured paper points out a great decrease in the volume of pores with 8 µm diameter, from 2.1 $cm^3 \cdot g^{-1}$ in the TMP sheet down to 1.3 $cm^3 \cdot g^{-1}$ in the z-layered structure. However, the pore volume of the pores around 1 µm in diameter does not show any difference when compared to the TMP sheet.

The values of porosity, specific surface, and mean pore diameter obtained from the MIP curves are presented in Table 1. As expected, the TMP sheet presented the highest porosity (76.3%) while the MNFC film presents the lowest porosity (55.3%). This last porosity value was higher than the one measured by González *et al.* (2014) due to the presence of the calcium carbonate filler in the MNFC suspension. As expected, the z-structured paper had a slightly lower porosity than the TMP sheet (74.5%). The specific surface values reveal the capacity of the MNFC film to develop a high specific surface (4.68 μm^{-1}) with a low mean pore diameter (0.47 µm). The addition of an MNFC layer of 6 $g \cdot m^{-2}$ increased significantly the paper specific surface from 1.08 μm^{-1} for the TMP sheet to 3.01 μm^{-1} for the z-structured paper. The reduction of the porosity and the increase of the specific surface of the z-structured paper lead to the significant decrease of the mean pore diameter of the paper, 0.99 µm compared to 2.83 µm for the TMP sheet.

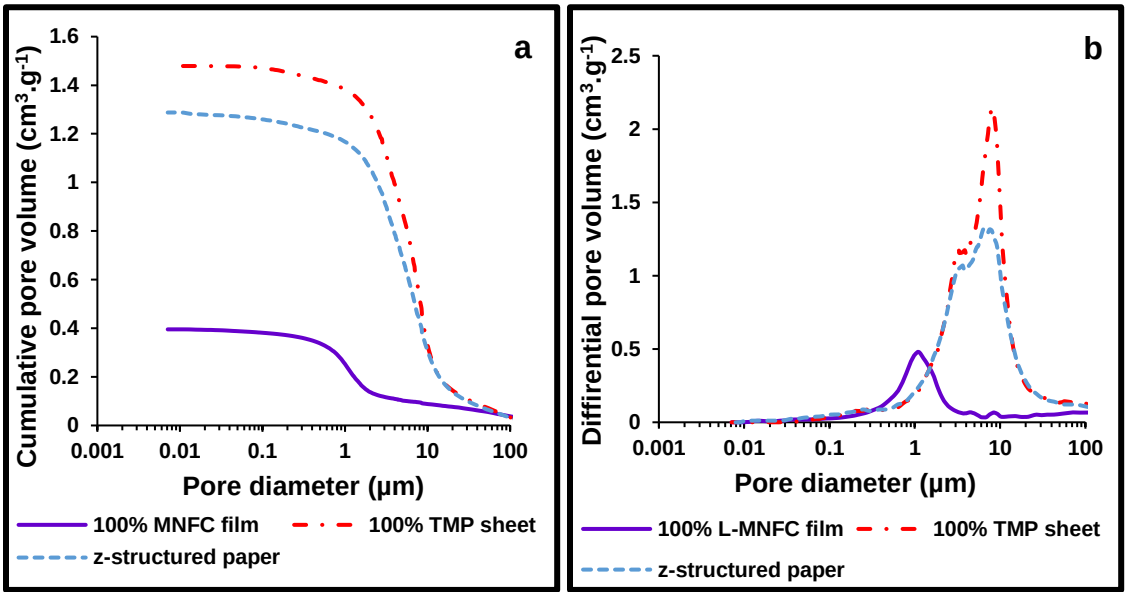

Fig. 1. Cumulative (a) and differential (b) pore volume of the paper samples

The MIP curves clearly demonstrate the change in the z-structured paper structure from the TMP sheet to the z-layered sheet, which confirms the retention of the MNFC layer in TMP sheet. However, these results do not provide any information about the MNFC layer position in the paper thickness. Furthermore, MIP results give only global

information about the structure, *i.e.* they do not allow to characterize the spatial structural difference between the surface structure and the paper bulk structure.

Table 1. Porosity, Specific Surface, and Mean Pore Diameter Calculated from MIP Curves

Sample	Porosity ε (%)	Specific surface S_v (μm^{-1})	Mean pore diameter Φ (µm)
100% MNFC film	55.3	4.68	0.47
100% TMP sheet	76.3	1.08	2.83
Z-structured paper	74.5	3.01	0.99

3D X-ray Synchrotron Microtomography

The SµT method enabled the characterization of the internal 3D paper structure. The 3D sample views presented in Fig. 2 show the differences between the TMP sheet and the MNFC film structure. In fact, the TMP sheet (Fig. 2a) displayed oriented thick fibers interwoven with fines. These fibers were oriented in the machine direction. The MNFC film (Fig. 2b) presented a denser structure with few small pores compared to the TMP sheet. MNFC fibrils appeared to be randomly oriented in the film structure. Obviously, the z-structured paper showed a similar TMP sheet surface structure, since the MNFC layer was added between two TMP layers (Fig. 2c). The paper section illustrates that the expected three-layer paper structure was indeed obtained: a shiny thin MNFC layer sandwiched between two TMP layers (Fig. 2d).

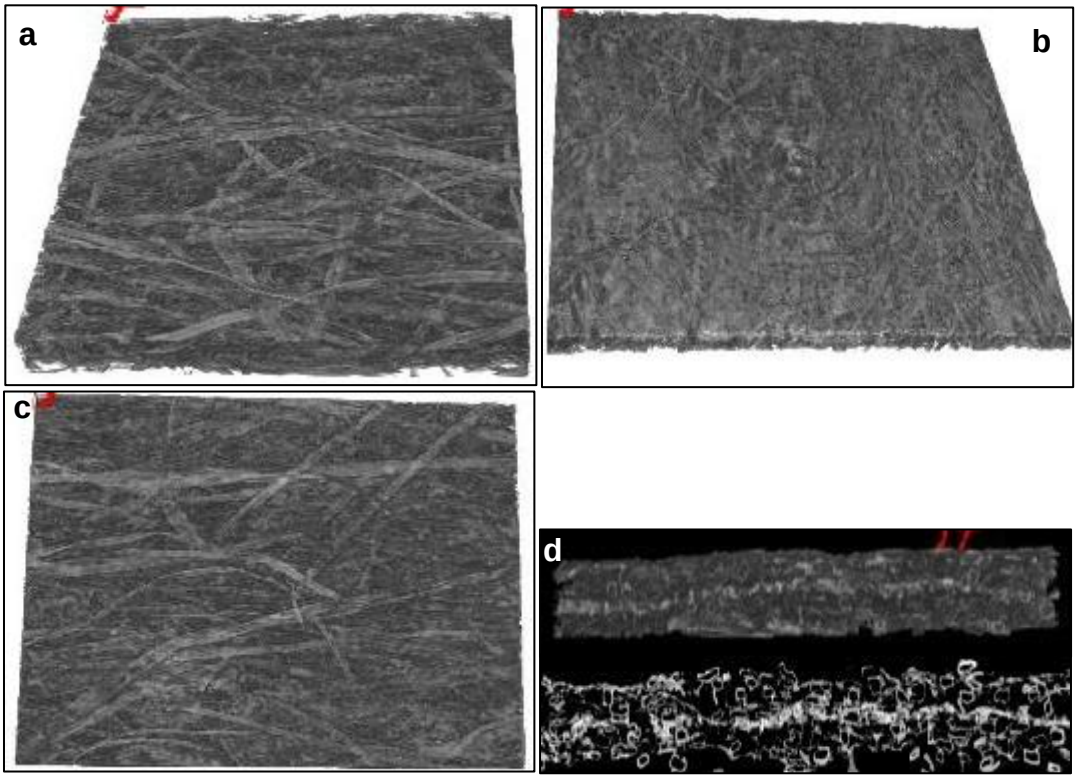

Fig. 2. 3D visualization of the studied samples: (a) 100% TMP sheet, (b) 100% MNFC film, (c) *z*-structured paper surface, and (d) z-structured paper thickness section

Table 2. Porosity, Specific Surface, and Mean Pore Diameter Calculated from the 3D Images

Sample	Porosity ε (%)	Specific surface S_v (μm^{-1})	Mean pore diameter Φ (µm)
100% MNFC film	40	2.6	0.6
100% TMP sheet	71	1.8	1.6
z-structured paper	63	2.4	1.0

From the 3D images, the calculated porosity and specific surface are presented in Table 2. As for the MIP results, the TMP sheet showed the highest porosity (71%), while the MNFC film presented the lowest porosity (40%). The addition of the MNFC layer reduced the z-structured paper porosity to 63%. The values of the porosity were lower than that obtained from MIP results. The difference can be explained by: (i) some mercury occlusion effect can be formed at the sample surface at low pressure, as explained by Ridgway and Gane (2003). When the pressure is increased, the occlusion is filled with mercury and is considered as paper porosity; (ii) some Post-it® adhesive used to fix the sample during the tomography measurement remains stuck to the sample and is considered as part of the sample structure in the 3D images. Considering the low Post-it® porosity, a lower overall porosity is obtained.

Besides previous general information about the difference in porosity between the different samples, 3D images offer the possibility to get additional information about the local variation of the porosity in the thickness of a given sample. The 100% TMP sheet and the 100% MNFC film porosity profiles along the paper thickness are presented in Fig. 3, which shows the expected typical profile shape of a monolayer paper structure (Rolland du Roscoat *et al.* 2008). The porosity decreased from the top surface to a constant plateau value of porosity, and it increased again upon reaching the bottom surface. Indeed, the plateau corresponded to the sheet bulk, whereas the varying parts were related to the top and bottom surface porosity, which in the present work is named *'3D roughness'*.

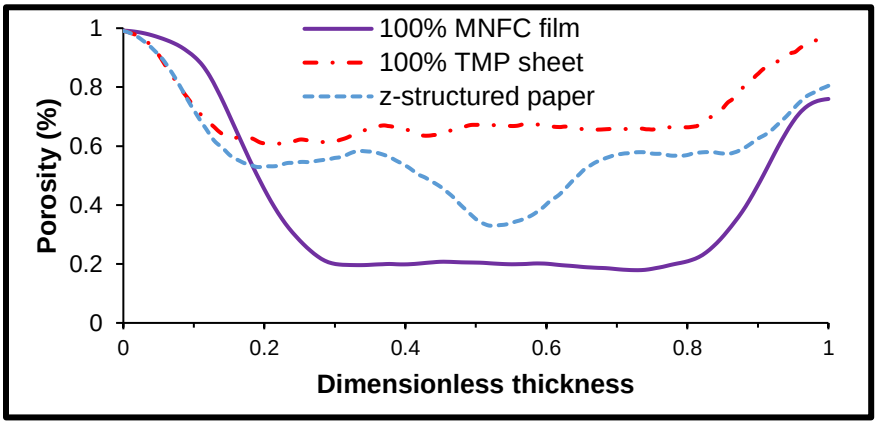

Fig. 3. Porosity profiles obtained from 3D data (SµT) among the normalized thickness of the papers defined as the current position divided the paper thickness

The porosity profile of the z-structured paper was quite different. It presented a non-constant porosity region in the middle of the bulk zone (at the same location of the former plateau) corresponding to the location of the MNFC layer in the paper thickness.

The porosity profile of the z-structured paper, with a lower porosity towards the middle of the sheet, confirms the retention of the MNFC layer at the targeted middle position of the paper thickness.

The porosity profiles in the thickness of the paper indicate that the global paper porosity is made up of two porosity regions: (i) the bulk porosity, which is almost constant, and (ii) the surface porosity, which increases at the surfaces of papers.

Considering such additional information, MIP results analysis can be improved to detect the bulk and surface porosity.

Improved MIP Analysis

To separate the surface and the bulk structures, the diameters of 10 and 3 µm were chosen as references for samples containing TMP fibers and only MNFC fibrils, respectively. The structural parameters were then recalculated from the MIP curves for the surface and the bulk structures. The results presented in Table 3 indicate, as expected, that most of the paper porosity originates from the bulk porosity. The surface porosity appears to be constant for the two papers. However, the bulk has a high developed specific surface when compared to the paper surface, leading to a reduced mean pore diameter in the bulk.

To validate such mathematical differentiation between the bulk and the surface structures, the bulk structure parameters were measured from the 3D tomography images. Results show that the bulk porosity values are very similar, almost the same, as the ones calculated by the improved MIP data analysis (Table 3).

Table 3. Surface and Bulk Porosity, Specific Surface, and Mean Pore Diameter Calculated from MIP Curves

Sample	MIP						SµT		
	Surface			Bulk			Bulk		
	ε (%)	S_v (μm^{-1})	Φ (µm)	ε (%)	S_v (μm^{-1})	Φ (µm)	ε (%)	S_v (μm^{-1})	Φ (µm)
100% MNFC film	18	0.1	5.4	25	8.0	0.1	21	2.7	0.3
100% TMP sheet	18	0.1	5.1	64	1.4	1.9	65	2.0	1.3
z-structured paper	17	0.2	3.4	57	4.8	0.4	51	2.5	0.8

Notes: ε: Porosity, S_v: Specific surface, Φ: Mean pore diameter)

CONCLUSIONS

Mercury intrusion porosimetry (MIP) is frequently used to characterize paper structure, but it only provides structural information, such as porosity or specific surface of the whole sheet, without the capability to differentiate between surface and bulk parameters. MIP does not provide any information about pores distribution in the paper structure. To overcome such limitations, 3D Synchrotron X-ray microtomography images were used to characterize both surface and bulk structures.

3D tomography images showed the presence of three zones in the porosity profile among the paper thickness. The zone of almost constant porosity positioned in the middle of the thickness represents the bulk porosity of the paper, and two zones of higher porosity. These last two regions correspond to boundary layers (roughness) positioned at each

surface of the sheet. From the results of the 3D tomography, MIP data were then divided in two parts using either 3 or 10 µm as the limit pore diameter value (depending on the sample composition) between the bulk and the surface. Pore diameters higher than 3 or 10 µm were considered to characterize the surface structure, in contrast to the bulk structure. The bulk porosity, calculated from MIP data, was found to be very similar to the bulk porosity measured from the 3D X-ray images, confirming the validity of the new approach.

REFERENCES CITED

Abell, A. B., Willis, K. L., and Lange, D. A. (1999). "Mercury intrusion porosimetry and image analysis of cement-based materials," *Journal of Colloid and Interface Science* 211(1), 39-44. DOI: 10.1006/jcis.1998.5986

Bloch, J.-F., and Kedadi, R. (2001). "Mercury intrusion technique: Structure analysis of porous media with porosity gradient," *Filtration & Separation* 38(5), 36-39. DOI: 10.1016/S0015-1882(01)80336-0

Bloch, J.-F., and Rolland du Roscoat, S. (2009). "Three-dimensional structural analysis," 14th Fundamental Research Symposium, Oxford, 599-664.

Brodin, F. W., Gregersen, O. W., and Syverud, K. (2014). "Cellulose nanofibrils: Challenges and possibilities as a paper additive or coating material—A review," *Nordic Pulp Paper Res*. J. 29(1), 156-166. DOI: 10.3183/NPPRJ-2014-29-01-p156-166

Charfeddine, M. A., Bloch, J.-F., Boller, E., and Mangin, P. (2016). "3D Synchrotron X-ray microtomography for paper structure characterization of z-structured paper by introducing micro nanofibrillated cellulose," *Nordic Pulp Paper Res. J*. 31(2), 218-223. DOI: 10.3183/NPPRJ-2016-31-02-p219-224

Considine, J. M., Vahey, D. W., Gleisner, R., Rudie, A., Du Roscoat, S. R., and Bloch, J.-F. (2010). "Z-direction fiber orientation in paperboard," *Tappi J*. 9(10), 25-32.

Dimic-Misic, K., Ridgway, C., Maloney, T., Paltakari, J., and Gane, P. (2014). "Influence on pore structure of micro/nanofibrillar cellulose in pigmented coating formulations," *Transport in Porous Media* 103(2), 155-179. DOI: 10.1007/s11242-014-0293-8

Giesche, H. (2006). "Mercury porosimetry: A general (practical) overview," *Particle & Particle Systems Characterization* 23(1), 9-19. DOI: 10.1002/ppsc.200601009

González, I., Alcalà, M., Chinga-Carrasco, G., Vilaseca, F., Boufi, S., and Mutjé, P. (2014). "From paper to nanopaper: Evolution of mechanical and physical properties," *Cellulose* 21(4), 2599-2609. DOI: 10.1007/s10570-014-0341-0

Hamada, H., Beckvermit, J., and Bousfield, D. W. (2010). "Nanofibrillated cellulose with fine clay as a coating agent to improve print quality," in: *TAPPI PaperCon Conference*, Atlanta, GA.

Holmstad, R., Goel, A., Ramaswamy, S., and Gregersen, O. W. (2006). "Visualization and characterization of high resolution 3D images of paper samples," *APPITA Journal* 59(5), 370.

Hyväluoma, J., Turpeinen, T., Raiskinmaki, P., Jasberg, A, Koponen, A., Kataja, M., Timonen, J., and Ramaswamy, S. (2007). "Intrusion of nonwetting liquid in paper," *Phys. Rev. E*. 75(3), Part: 2. Article 036301.

Johnson, R. W., Abrams, L., Maynard, R. B., and Amick, T. J. (1999). "Use of mercury porosimetry to characterize pore structure and model end-use properties of coated papers-Part I: Optical and strength properties," *TAPPI Journal* 82(1), 239-251.

Moura, M., and Figueiredo, M. (2002). "Characterization of eucalypt wood by mercury porosimetry – Data interpretation," *Bull. Mocrom. Industr. Corp*. 13(5), 8-9.

Moura, M. J., Ferreira, P. J., and Figueiredo, M. M. (2005). "Mercury intrusion porosimetry in pulp and paper technology," *Powder Technology* 160(2), 61-66. DOI: 10.1016/j.powtec.2005.08.033

Münch, B., and Holzer, L. (2008). "Contradicting geometrical concepts in pore size analysis attained with electron microscopy and mercury intrusion," *J. Am. Ceram. Soc*. 91(12), 4059-4067. DOI: 10.1111/j.1551-2916.2008.02736.x

Ridgway, C. J., and Gane, P. A. (2003). "Bulk density measurement and coating porosity calculation for coated paper samples," *Nordic Pulp and Paper Research Journal* 18(1), 24-31. DOI: 10.3183/NPPRJ-2003-18-01-p024-031

Ridgway, C. J., and Gane, P. A. (2013). "Size-selective absorption and adsorption in anionic pigmented porous coating structures: Case study cationic starch polymer versus nanofibrillated cellulose," *Cellulose* 20(2), 933-951. DOI: 10.1007/s10570-013-9878-6

Rolland du Roscoat, S., Bloch, J. F., and Caulet, P. (2012). "A method to quantify the 3D microstructure of fibrous materials containing mineral fillers using X-ray microtomography: Application to paper materials," *Journal of Materials Science* 47(18), 6517-6521. DOI: 10.1007/s10853-012-6575-z

Rolland du Roscoat, S., Bloch, J. F., and Thibault, X. (2005). "Synchrotron radiation microtomography applied to investigation of paper," *Journal of Physics D: Applied Physics* 38(10A), A78-A84. DOI: 10.1088/0022-3727/38/10A/015

Rolland du Roscoat, S., Decain, M., Geindreau, C., Thibault, X., and Bloch, J.-F. (2008). "Microstructural analysis of paper using synchrotron X-ray microtomography: Numerical estimation of the permeability and effective thermal conductivity," *APPITA Journal* 61(4), 286.

Rootare, H. M., and Prezlow, C. F. (1967). "Surface areas from mercury porosimetry measurements," *J. Phys. Chem*., 2733-2736. DOI: 10.1021/j100867a057

Yamauchi, T. (2007). "A method to determine lumen volume and collapse degree of pulp fibers by using bottleneck effect of mercury porosimetry," *Journal of Wood Science* 53(6), 516-519. DOI: 10.1007/s10086-007-0895-7

Zauer, M., Hempel, S., Pfriem, A., Mechtcherine, V., and Wagenführ, A. (2014). "Investigations of the pore-size distribution of wood in the dry and wet state by means of mercury intrusion porosimetry," *Wood Science and Technology* 48(6), 1229-1240. DOI: 10.1007/s00226-014-0671-y

Article submitted: February 2, 2017; Peer review completed: March 26, 2017; Revised version received and accepted: January 10, 2019; Published: February 13, 2019.
DOI: 10.15376/biores.14.2.2642-2650